Electronic Research Archive

https://www.aimspress.com/journal/era

ERA, 34(7): 5040–5061.
DOI: 10.3934/era.2026223
Received: 30 April 2026
Revised: 25 May 2026
Accepted: 05 June 2026
Published: 10 June 2026

Research article

Cross-regional theta–beta phase–amplitude coupling between cortex and globus pallidus internus: A computational study

Bei Bai[1] **and Xia Shi**[1,2,*]

[1] School of Mathematical Sciences, Beijing University of Posts and Telecommunications, Beijing 100876, China

[2] Key Laboratory of Mathematics and Information Networks (Beijing University of Posts and Telecommunications), Ministry of Education, Beijing 100876, China

* **Correspondence:** Email: shixiabupt@163.com.

Abstract: In Parkinson's disease (PD), abnormal oscillations pervade the cortex–basal ganglia–thalamus (CTX-BG-Th) loop. In recent years, more and more evidence has shown the physiological phenomena of exaggerated phase–amplitude coupling (PAC) in PD, suggesting that such coupling contributes to the generation and propagation of pathological oscillations. However, current understanding of how cortical low-frequency rhythms shape downstream pathological activity is still incomplete. In this study, we aim to investigate how the theta-band (3–9 Hz) phase of layer 5 pyramidal tract (E5P) cortical neurons modulates the beta-band (13–30Hz) amplitude of globus pallidus internus (GPi) neurons. The modulation index (MI), time-lag MI analysis, and coherence analysis are introduced to quantify the strength, temporal characteristics, and pathway dependence of PAC. The results indicate that significant cross-regional θ–β PAC occurs between E5P and GPi in the PD state, and this coupling has time delay characteristics and mainly relies on indirect pathways. In addition, blocking indirect pathways or reducing the θ power of E5P will decrease the β oscillation of GPi. These findings elucidate the dynamic mechanism of cortical regulation of GPi related oscillations, providing a theoretical basis for targeted interventions in PD patients through cortical modulation.

Keywords: phase–amplitude coupling; basal ganglia; cortex; oscillation; Parkinson's disease

1. Introduction

The basal ganglia (BG) is a group of interconnected subcortical nuclei that plays essential roles in motor control, action selection, and reward-based learning [1, 2]. Among BG nuclei, the internal segment of the globus pallidus (GPi) serves as the principal output nucleus and exerts tonic inhibitory control over the thalamus [3, 4]. Abnormal GPi activity can contribute to motor dysfunction.

In Parkinson's disease (PD), degeneration of dopaminergic neurons gives rise to abnormal oscillatory activity throughout the BG network. Previous studies have shown that exaggerated beta-band (13–30 Hz) oscillations in GPi are closely associated with the PD state [5–7]. In particular, elevated beta-band oscillatory activity is associated with bradykinesia and rigidity, and clinical interventions commonly adopt pharmacotherapy or deep brain stimulation (DBS) [8, 9]. Despite the extensive studies on β oscillations, growing evidence suggests that pathological BG dynamics cannot be fully explained by β power alone. Instead, interactions across multiple frequency bands may also play an important role in shaping abnormal network activity. A key factor in this perspective is cortical input. The cerebral cortex (CTX), especially the primary motor cortex, provides the major excitatory drive to the BG. Classically, cortical signals reach GPi through three major pathways: the direct pathway (CTX→D1-type medium spiny neuron (D1-MSN)→GPi), the indirect pathway (CTX→D2-type medium spiny neuron (D2-MSN)→the external segment of the globus pallidus (GPe)→subthalamic nucleus (STN)→GPi), and the hyperdirect pathway (CTX→STN→GPi) [10, 11].

Phase–amplitude coupling (PAC) provides a natural framework for describing interactions between neural rhythms at different frequencies. In PAC, the phase of a low-frequency oscillation modulates the amplitude of a higher-frequency oscillation [12, 13]. To quantify this phenomenon, Tort et al. [14] introduced the modulation index (MI), an information-theoretic measure based on Kullback–Leibler (KL) divergence, which has since become a standard tool for PAC analysis. In recent years, PAC has been widely observed in experimental studies of both healthy and pathological brain activity. In Parkinson's disease, abnormal PAC has been observed in cortical and subcortical circuits and is thought to reflect pathological interactions across temporal scales. For example, de Hemptinne et al. [15] reported exaggerated beta-broadband gamma PAC in the motor cortex of PD patients, and further showed that this abnormal coupling can be reduced by STN-DBS [16]. At the inter-regional level, Zheng et al. [17] showed that amygdala θ/α phase modulates hippocampal high-γ amplitude, and Nandi et al. [18] proposed a directional inter-regional PAC framework to infer the direction of rhythmic signal transmission between brain regions. These studies suggest that PAC is not only a local electrophysiological phenomenon, but also a potential mechanism for cross-region signal transmission and pathological rhythm coordination.

Beyond experimental observations, PAC has also been increasingly studied from the perspective of neural dynamics and computational modeling. Such studies are useful because they can isolate pathway-specific effects and reveal the dynamical mechanisms that are difficult to test directly in experiments. Within the BG system, Yu et al. [19] constructed a CTX-BG-thalamus (Th) network model and showed that β-γ PAC is enhanced in the Parkinsonian state [20], supporting the idea that cortical rhythms can influence pathological BG activity. However, existing studies have mainly focused on local PAC, near-neighbor inter-regional PAC, or same-frequency oscillatory propagation along BG pathways. The role of deep cortical low-frequency rhythms in shaping downstream pathological beta activity of GPi through cross-regional, cross-frequency interactions remains insufficiently understood. In particular, there is still a lack of systematic investigation into how the theta-band activity of deep cortical neurons modulates GPi beta oscillations and through which pathways this modulation is realized. These issues motivate the present study.

Importantly, we focus on the θ band, and several observations point to a possible role of cortical θ activity. Layer 5 pyramidal tract (PT) neurons can exhibit prominent theta-band activity [21, 22]. Our previous studies showed that cortical intrinsic dynamics exert frequency-selective influences on

GPi oscillations [23]. Cortical theta has been implicated in long-range top-down coordination across brain regions [24, 25]. Taken together, these observations raise a specific possibility: The θ phase of deep-layer cortical output neurons may modulate the pathological β amplitude of GPi neurons.

This study focuses on excitatory layer 5 pyramidal neurons (E5P) and examines whether their θ rhythm modulates GPi β oscillations in the PD state. To address this issue, we employ a layered CTX-BG-Th network model and investigate three related questions: whether the theta-band phase of E5P exhibits significant phase–amplitude coupling with the beta-band amplitude of GPi under PD conditions, whether this coupling shows pathway dependence and temporal directionality, and whether modulation of cortical theta activity can attenuate pathological β oscillations in GPi. The remainder of this article is organized as follows. Section 2 presents the construction of the CTX-BG-Th network model, including the neuron models, synaptic connectivity, and analytical methods used in this study. Section 3 reports the main findings, including the dynamical characteristics of the network in the PD state, the identification of cross-regional θ–β coupling between E5P and GPi, the pathway- and delay-dependent analyses of this coupling, and the effects of cortical-theta-based interventions on pathological GPi β activity. Section 4 summarizes the principal conclusions and discusses their mechanistic and potential therapeutic implications.

2. Materials and methods

2.1. Network model

The CTX-BG-Th network model is constructed by coupling a layered cortical model with a biophysically detailed BG-thalamus model [19,26–28]. Due to the fewer neurons in the first and fourth layers of the motor cortex, and the fact that cortical thalamic neurons in the sixth layer mainly project to the thalamus, we did not consider modeling these layers [27,29]. The cortical model includes layer 2/3 and layer 5. Eight neuronal populations are modeled: E23, intratelencephalic (IT) excitatory neurons in layer 2/3; I23, parvalbumin (PV) inhibitory neurons in layer 2/3; I23L, somatostatin-expressing (SOM) inhibitory neurons in layer 2/3; E5A and E5B, IT excitatory neurons in layers 5A and 5B, respectively; E5P, pyramidal tract (PT) excitatory neurons in layer 5B; I5, PV inhibitory neurons in layer 5; and I5L, SOM inhibitory neurons in layer 5 [30].

The BG model comprises D1-type medium spiny neurons (D1-MSN) and D2-type medium spiny neurons (D2-MSN) in the striatum (Str), subthalamic nucleus (STN) neurons, external globus pallidus (GPe) neurons, and GPi neurons. The population sizes used in the network are listed in Table 1 [19].

Table 1. Neuron population sizes used in the network.

CTX		BG and Th	
Population	Number	Population	Number
E23	218	D1-MSN	100
I23	30	D2-MSN	100
I23L	30	GPe	100
E5A	126	GPi	100
E5B	144	STN	100
E5P	144	Th	100
I5	66		
I5L	66		

Three pathways connect the cortex to GPi. The direct pathway: E5A→D1-MSN→GPi. The indirect pathway: E5P→D2-MSN→GPe→STN→GPi. The hyperdirect pathway: E5P→STN→GPi. A schematic of the network architecture is shown in Figure 1, and the cortical layered structure is shown in Figure 2.

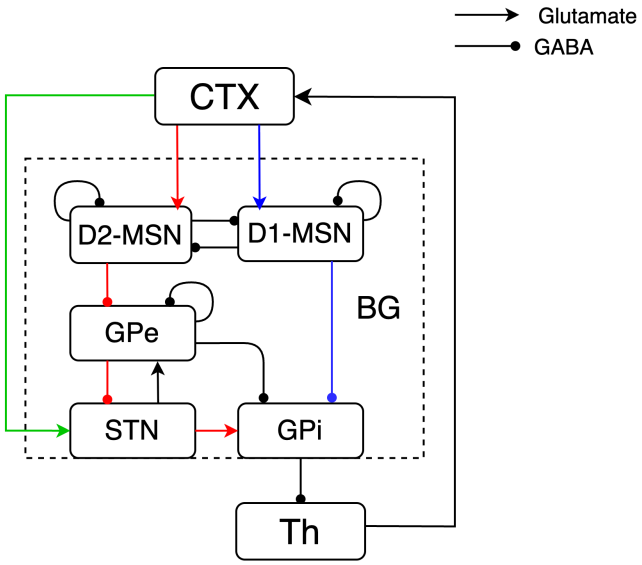

Figure 1. Schematic diagram of the CTX-BG-Th network model. The blue pathway represents the direct pathway, the red pathway symbolizes the indirect pathway, and the green pathway denotes the hyperdirect pathway. Excitatory connections are shown as arrows and inhibitory connections as circles.

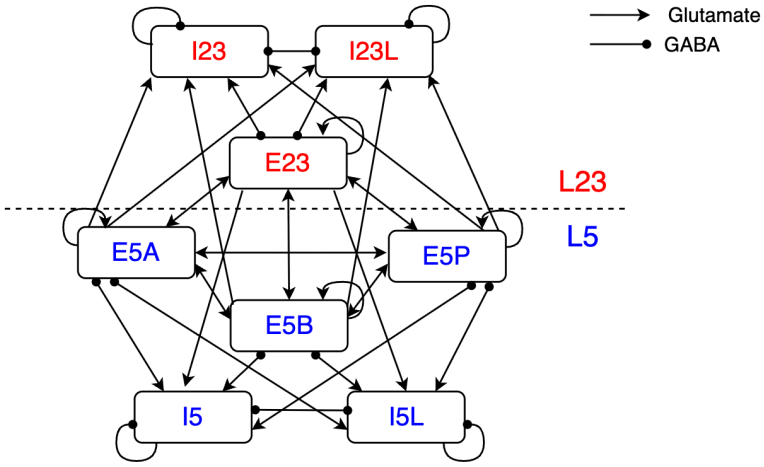

Figure 2. Layered structure of the cortical model. The cortex comprises layer 2/3 and layer 5. Eight populations are included: E23, I23, I23L in layer 2/3 and E5A, E5B, E5P, I5, I5L in layer 5.

2.2. Individual neuron model

(i) Cortical neurons

All cortical neurons are modeled as single-compartment Hodgkin–Huxley (H-H)-type neurons following Pospischil et al. [30, 31]. The membrane equation is specified as:

$$C_m \frac{\mathrm{d}V}{\mathrm{d}t} = -I_L - I_{Na} - I_K - I_M - I_{\text{ion}} - I_{\text{syn}} + I_{\text{app}}, \tag{2.1}$$

where $C_m = 1\ \mu\text{F/cm}^2$ is the membrane capacitance, I_L is the leak current, I_{Na} is the fast sodium current, I_K is the delayed rectifier potassium current, I_M is the slow noninactivating potassium current responsible for spike-frequency adaptation, I_{ion} represents additional ionic currents specific to each cell type, I_{syn} is the total synaptic current, and I_{app} is the applied current. I_{app} includes a constant direct-current component together with a stochastic background component, which was implemented as discrete-time Gaussian white noise. This stochastic component is used to approximate background synaptic fluctuations and nonspecific inputs from cortical components that are not explicitly modeled. Therefore, although the cortical architecture is simplified, the model still retains background variability in the cortical neuronal dynamics.

Specifically, we use regular-spiking (RS), fast-spiking (FS), low-threshold spike (LTS), and internally burning (IB) cells to simulate IT, PV, SOM, and PT neurons, respectively. For RS and FS, these neurons contain I_L, I_{Na}, I_K, and I_M. No additional ionic current: $I_{\text{ion}} = 0$. For IB and LTS, these neurons also include a high-threshold L-type calcium current I_{Ca} [32, 33]: $I_{\text{ion}} = I_{Ca}$.

(ii) BG and Th neurons

The models for BG and Th follow Kumaravelu et al. [28, 34, 35]. The membrane potential of each cell is specified as:

$$\begin{aligned} C_m \cdot \frac{\mathrm{d}v_{D1-MSN}}{\mathrm{d}t} = &- I_l - I_K - I_{Na} - I_m - I_{gaba} - I_{e-CTX\to D1-MSN} \\ &- I_{D2-MSN\to D1-MSN} + I_{appD1}, \end{aligned} \tag{2.2}$$

$$\begin{aligned} C_m \cdot \frac{\mathrm{d}v_{D2-MSN}}{\mathrm{d}t} = &- I_l - I_K - I_{Na} - I_m - I_{gaba} - I_{e-CTX\to D2-MSN} \\ &- I_{D1-MSN\to D2-MSN} + I_{appD2}, \end{aligned} \tag{2.3}$$

$$\begin{aligned} C_m \cdot \frac{\mathrm{d}v_{STN}}{\mathrm{d}t} = &- I_l - I_K - I_{Na} - I_a - I_L - I_t - I_{Cak} \\ &- I_{GPe\to STN} - I_{e-CTX\to STN,ampa} \\ &- I_{e-CTX\to STN,nmda} + I_{appSTN}, \end{aligned} \tag{2.4}$$

$$\begin{aligned} C_m \cdot \frac{\mathrm{d}v_{GPe}}{\mathrm{d}t} = &- I_l - I_K - I_{Na} - I_t - I_{Ca} - I_{ahp} \\ &- I_{STN\to GPe,ampa} - I_{STN\to GPe,nmda} - I_{GPe\to GPe} \\ &- I_{D2-MSN\to GPe} + I_{appGPe}, \end{aligned} \tag{2.5}$$

$$C_m \cdot \frac{\mathrm{d}v_{GPi}}{\mathrm{dt}} = -I_l - I_K - I_{Na} - I_t - I_{Ca} - I_{ahp} - I_{STN\to GPi,ampa} - I_{GPe\to GPi} - I_{D1-MSN\to GPi} + I_{appGPi}, \tag{2.6}$$

$$C_m \cdot \frac{\mathrm{d}v_{Th}}{\mathrm{dt}} = -I_l - I_K - I_{Na} - I_t - I_{GPi\to Th} + I_{appTh}. \tag{2.7}$$

2.3. Synaptic models

The three conductance-based chemical synaptic currents are selected according to the neurotransmitter type and the characteristic time scale of each pathway, following previous CTX-BG-Th network models [28, 36–41]. The synaptic current from neuron x to neuron y is

$$I_{x\to y}(t) = g_{x\to y}\,(V_y(t) - E_{\mathrm{syn}})\,s(t), \tag{2.8}$$

where $g_{x\to y}$ is the maximal synaptic conductance, E_{syn} is the reversal potential (0 mV for excitatory, −80 mV for inhibitory), and $s(t)$ is the synaptic gating variable.

Alpha synapse. This form is used for the synapses in the cortical microcircuit and for fast cortical glutamatergic projections to the Str. These connections include intracortical excitatory and inhibitory synapses as well as E5A→D1-MSN and E5P→D2-MSN corticostriatal projections:

$$s(t) = \bar{g}_{\mathrm{syn}} \frac{t - t_d}{\tau} \exp\left(-\frac{t - t_d}{\tau}\right). \tag{2.9}$$

Single-exponential synapse. This form is used for gamma-aminobutyric acid (GABA)ergic inhibitory projections with relatively simple decay dynamics, including recurrent and collateral inhibition within the Str, MSN→GP, GP→GPe, GPe→GPi, and GPi→Th projections:

$$s(t) = \bar{g}_{\mathrm{syn}} \exp\left(-\frac{t - t_d}{\tau}\right). \tag{2.10}$$

Bi-exponential synapse. This form is used for synapses with distinct rise and decay phases, including the glutamatergic AMPA-mediated excitatory projections STN→GPe, STN→GPi, and E5P→STN as well as the GABAergic inhibitory projection GPe→STN.

$$s(t) = \bar{g}_{\mathrm{syn}} \cdot h \left[\exp\left(-\frac{t - t_d}{\tau_d}\right) - \exp\left(-\frac{t - t_d}{\tau_r}\right)\right], \tag{2.11}$$

where τ_r and τ_d are the rise and decay time constants, and h is a normalization factor ensuring unit peak amplitude. Simulations were implemented by the forward Euler method with a time step of 0.01 ms.

The detailed synaptic connectivity within the CTX-BG-Th network is listed in Tables 2 and 3.

Table 2. Synaptic connectivity within the cortical microcircuit. Connection probability p and effective maximal conductance $g_{\max}$ (mS/cm^2) are listed. All connections use fixed-probability random wiring.

Connection	p	$g_{\max}$	Connection	p	$g_{\max}$
Post: E23			*Post: I23*		
E23→E23	0.15	0.0024	E23→I23	0.19	0.0023
I23→E23	1.00	0.0024	I23→I23	1.00	0.0020
I23L→E23	1.00	0.0021	I23L→I23	1.00	0.0006
E5A→E23	0.04	0.0020	E5A→I23	0.02	0.0011
E5B→E23	0.02	0.0009	E5B→I23	0.02	0.0011
			E5P→I23	0.02	0.0011
Post: E5A			*Post: I23L*		
E23→E5A	0.10	0.0036	E23→I23L	0.19	0.0023
E5A→E5A	0.18	0.0020	I23→I23L	1.00	0.0020
E5B→E5A	0.18	0.0012	I23L→I23L	1.00	0.0006
I5→E5A	1.00	0.0024	E5A→I23L	0.02	0.0011
I5L→E5A	1.00	0.0021	E5B→I23L	0.02	0.0011
			E5P→I23L	0.02	0.0011
Post: E5B			*Post: I5*		
E23→E5B	0.05	0.0034	E23→I5	0.02	0.0003
E5A→E5B	0.01	0.0032	E5A→I5	0.19	0.0032
E5B→E5B	0.05	0.0024	E5B→I5	0.19	0.0032
I5→E5B	1.00	0.0024	E5P→I5	0.19	0.0032
I5L→E5B	1.00	0.0021	I5→I5	1.00	0.0020
			I5L→I5	1.00	0.0006
Post: E5P			*Post: I5L*		
E23→E5P	0.11	0.0042	E23→I5L	0.22	0.0030
E5A→E5P	0.02	0.0042	E5A→I5L	0.03	0.0032
E5B→E5P	0.04	0.0034	E5B→I5L	0.03	0.0032
E5P→E5P	0.18	0.0034	E5P→I5L	0.03	0.0032
I5→E5P	1.00	0.0020	I5→I5L	1.00	0.0020
I5L→E5P	1.00	0.0005	I5L→I5L	1.00	0.0006

Table 3. Synaptic connectivity between CTX, BG, and Th. Connection probability p and effective maximal conductance $g_{\max}$ (mS/cm^2) are listed.

Connection	p	$g_{\max}$	Connection	p	$g_{\max}$
CTX → BG			*BG output → Th*		
E5A→D1-MSN	0.60	0.0100	GPi→Th	1–1	0.0700
E5P→D2-MSN	0.50	0.0030			
E5P→STN	0.20	0.0500			
BG internal			*Feedback → CTX*		
D1-MSN→D1-MSN	0.70	0.0004	STN→E23	0.50	0.0004
D2-MSN→D1-MSN	0.70	0.0002	STN→I23	0.50	0.0004
D2-MSN→D2-MSN	0.70	0.0004	STN→I23L	0.50	0.0004
D1-MSN→GPi	0.70	0.1300	Th→E23	0.20	0.0004
D2-MSN→GPe	1.00	0.0300	Th→E5A	0.20	0.0004
STN→GPi	0.60	0.0225	Th→E5B	0.20	0.0004
GPe→GPi	0.40	0.0880	Th→E5P	0.20	0.0004
STN→GPe	0.30	0.0023			
GPe→GPe	0.50	0.0360			
GPe→STN	0.60	0.0400			

2.4. Methods

(i) Phase-amplitude coupling analysis

Cross-regional PAC between E5P θ phase and GPi β amplitude is quantified using the modulation index (MI) of Tort et al. [14]. Specifically, MI is used to determine whether the θ phase of E5P neurons modulates the β amplitude of GPi neurons, thereby characterizing the strength of cross-regional cross-frequency coupling. The procedure as follows:

1) Bandpass filter the E5P signal in the theta range (3–9 Hz) to obtain $x_{\mathrm{E5P},\theta}(t)$.
2) Bandpass filter the GPi signal in the beta range (13–30 Hz) to obtain $x_{\mathrm{GPi},\beta}(t)$.
3) Apply the Hilbert transform to extract the instantaneous phase $\phi_{\mathrm{E5P},\theta}(t)$ and the amplitude envelope $A_{\mathrm{GPi},\beta}(t)$.
4) Divide $\phi_{\mathrm{E5P},\theta}(t)$ into $N = 18$ equally spaced phase bins covering $[0, 2\pi)$.
5) For each bin j, compute the mean beta amplitude $\langle A_{\mathrm{GPi},\beta}\rangle_j$.
6) Normalize to obtain a probability-like distribution:

$$P(j) = \frac{\langle A_{\mathrm{GPi},\beta}\rangle_j}{\sum_{k=1}^{N}\langle A_{\mathrm{GPi},\beta}\rangle_k}. \tag{2.12}$$

The MI is defined as:

$$\mathrm{MI} = \frac{D_{\mathrm{KL}}(P\|U)}{\log N} = \frac{\sum_{j=1}^{N} P(j)\log\dfrac{P(j)}{1/N}}{\log N}, \tag{2.13}$$

where U is the uniform distribution. The MI ranges from 0 (no coupling) to 1 (maximal coupling).

To assess temporal directionality, we compute the MI at varying time lags τ:

$$\mathrm{MI}(\tau) = \mathrm{MI}\Big(\phi_{\mathrm{E5P},\theta}(t),\ A_{\mathrm{GPi},\beta}(t+\tau)\Big), \tag{2.14}$$

where τ is scanned from -100 to $+100$ ms. If the MI peak occurs at $\tau > 0$, the E5P theta phase leads the GPi β amplitude change. This supports the hypothesis of descending CTX modulation. If the peak occurs at $\tau = 0$, only simultaneous coupling is indicated. A peak at $\tau < 0$ would not support CTX-to-GPi transmission.

(ii) Beta coherence

The coherence between E5P and GPi signals is defined as:

$$C_{xy}(f) = \frac{|P_{xy}(f)|^2}{P_{xx}(f)\,P_{yy}(f)}, \tag{2.15}$$

where $P_{xx}(f)$ and $P_{yy}(f)$ are the autopower spectra of E5P and GPi, respectively, and $P_{xy}(f)$ is the cross-power spectrum. $C_{xy}(f)$ ranges from 0 to 1. A scalar beta-band coherence is obtained by averaging over 13–30 Hz:

$$\overline{C}_\beta = \frac{1}{|N_\beta|}\sum_{f\in[13,30]\,\mathrm{Hz}} C_{xy}(f), \tag{2.16}$$

where $|N_\beta|$ is the number of frequency bins in the beta band.

(iii) Statistical analysis

All quantitative comparisons were performed across 10 independent simulation trials with paired random seeds. For each paired comparison, the same random seed was used under the two compared conditions so that the statistical test reflected the effect of the model condition rather than differences in stochastic initialization. Data are shown as mean standard deviation or as box plots. Two-tailed paired Student's t-tests were used for pairwise comparisons, and $p < 0.05$ was considered statistically significant.

3. Results

3.1. Dynamical properties of the network in the PD state

The PD state is simulated by modifying key parameters to reflect dopamine depletion. The parameter modifications are listed in Table 4. Figures 3 and 4 show the membrane potential traces of neurons in the CTX-BG-Th network under PD conditions. The PSD comparison between normal and PD states quantitatively confirms these observations (Figure 5). In the PD state, the GPi PSD reveals a prominent spectral peak within the beta band, whereas no dominant oscillatory peak is detected in the normal state, which is consistent with experimental observations in dopamine-depleted states [42, 43].

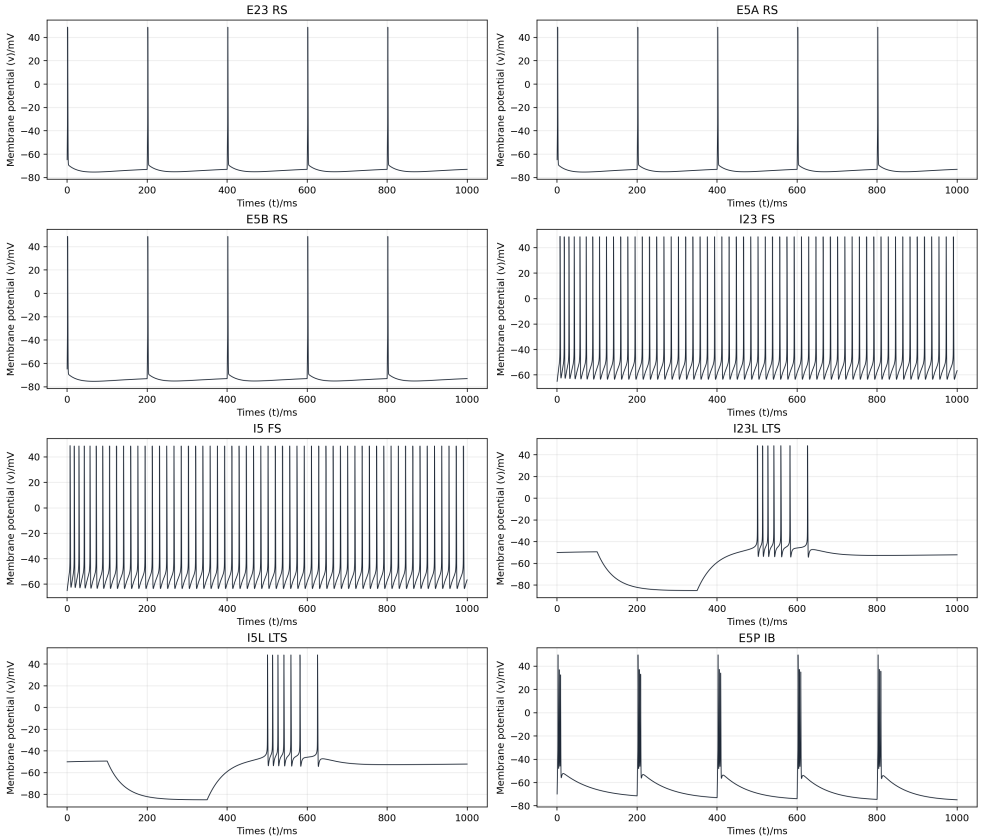

Figure 3. Membrane potential traces of CTX neurons under the PD condition.

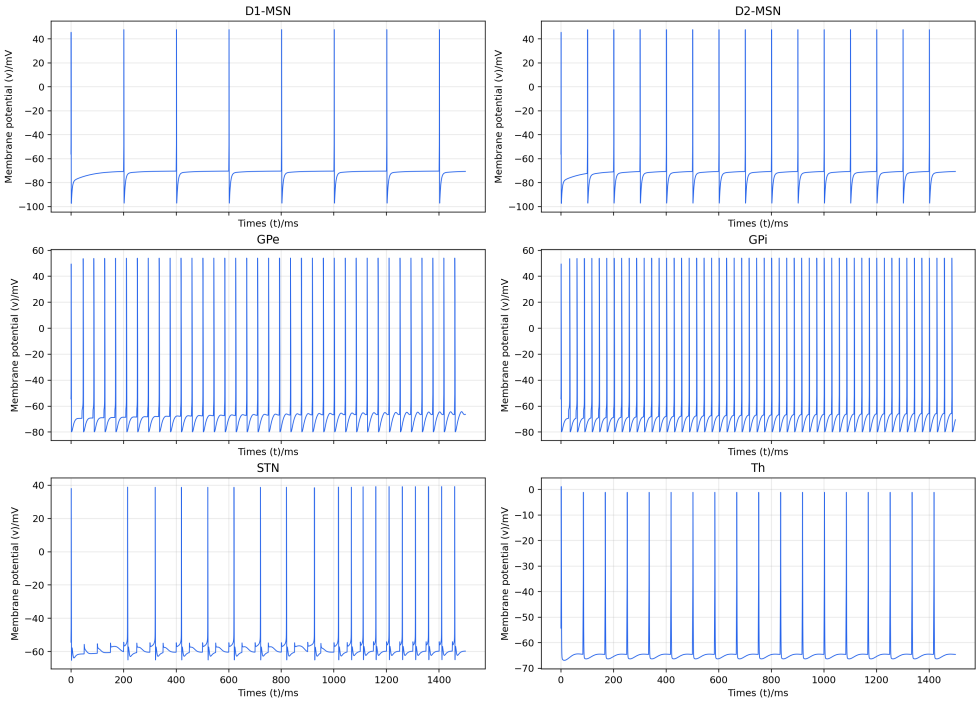

Figure 4. Membrane potential traces of BG and Th neurons under the PD condition.

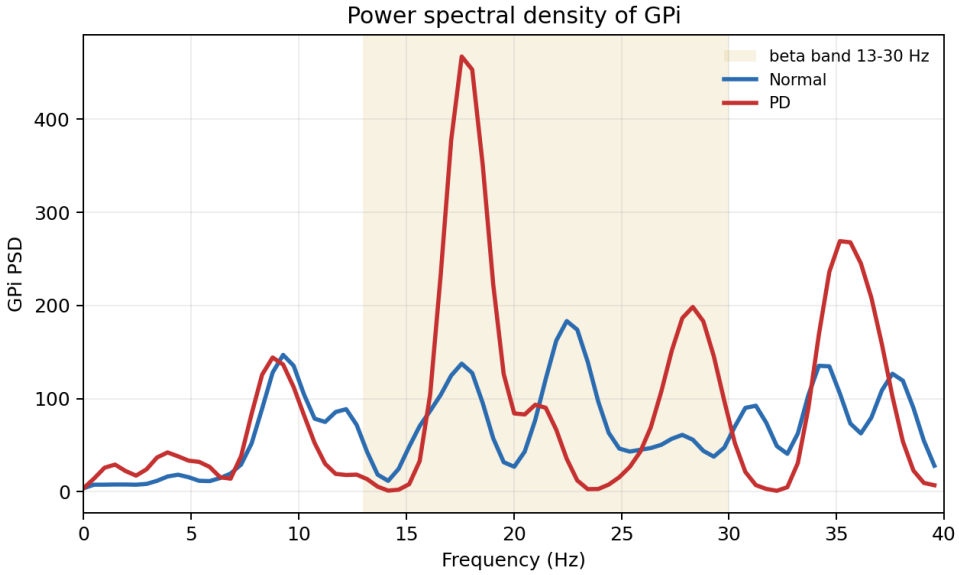

Figure 5. PSD of GPi neurons under normal (blue) and PD (red) conditions. The shaded region marks the beta band (13–30 Hz).

Table 4. Parameter modifications for PD simulation.

Parameter	Normal	PD	Parameter	Normal	PD
D1-MSN→D1-MSN g_{max}	2.60	2.25	GPe→GPi g_{max}	0.080	0.088
D2-MSN→D2-MSN g_{max}	2.60	2.25	GPe→GPe g_{max}	0.009	0.036
D1-MSN→GPi g_{max}	0.100	0.130	E5A→D1-MSN g_{max}	0.0269	0.010
STN→GPi g_{max}	0.050	0.0225	E5P→LTS g_{max}	0.0018	0.00045

To further justify the choice of cortical phase source for the subsequent PAC analysis, we compared the theta-band power (3–9 Hz) of E5A and E5P across 10 paired simulation trials, two cortical populations all that project to the basal ganglia (Figure 6). Under the PD state, E5A shows only a limited change in θ power ($p = 0.160$), whereas E5P displays a much more pronounced θ enhancement ($p = 0.001$). Accordingly, we selected E5P rather than E5A as the cortical phase source in the following cross-regional PAC analysis. This provides the spectral basis for examining whether the theta phase of E5P modulates the beta-band amplitude of GPi in a cross-regional manner.

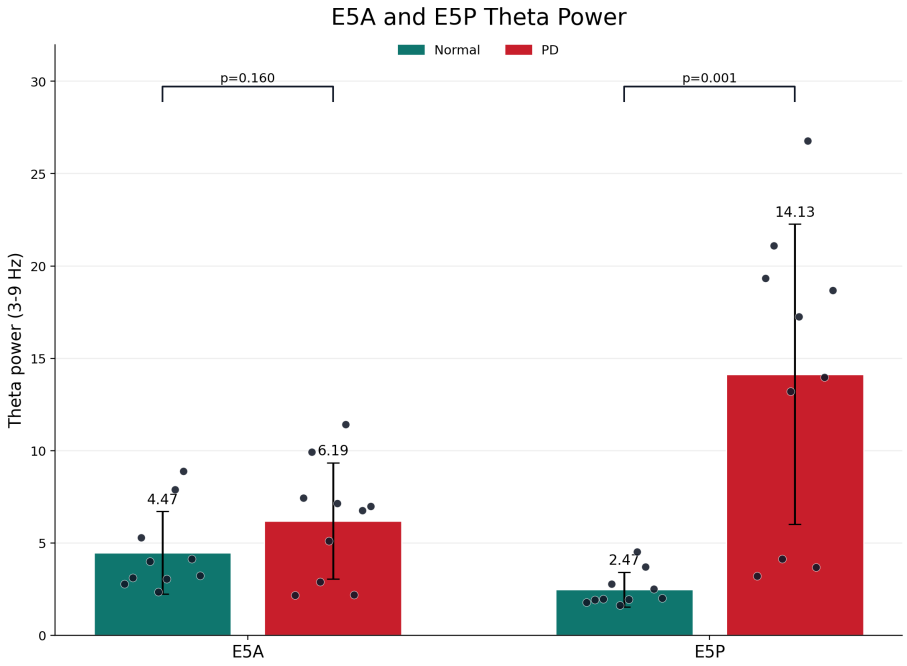

Figure 6. Theta-band power of E5A and E5P under normal (green) and PD (red) conditions.

3.2. Cross-regional θ–β PAC between E5P and GPi

We next quantify the cross-regional PAC between E5P θ phase and GPi β amplitude. Unlike conventional local PAC analyses that examine coupling within a single nucleus, this analysis targets interstructure coupling: The phase is extracted from cortical E5P neurons, and the amplitude is extracted from GPi neurons in the BG output. This cross-regional, cross-frequency measure probes whether the temporal structure of CTX θ oscillations organizes the expression of pathological β activity in a downstream nucleus.

Figure 7(a) presents the comodulogram for both conditions. In the normal state, the comodulogram

shows relatively diffuse MI values. The peak MI is 0.0122, located at 4.5 Hz (phase) / 19.0 HZ (amplitude). No concentrated hot spot is visible. In the PD state, the pattern changes qualitatively. A distinct hot spot emerges, with a peak MI of 0.0164 at 5.5 Hz (phase) / 25.0 Hz (amplitude). The bar chart in Figure 7(b) further quantifies this difference. We compared the fixed-band MI between the normal and PD conditions across 10 paired simulation trials. The mean θ–β MI across the region of interest (ROI) increases from approximately 0.002 in the normal state to approximately 0.0045 in the PD state ($p = 0.038$). This result confirms that the cross-regional θ–β PAC is selectively enhanced in the PD state, supporting the hypothesis that cortical θ activity contributes to the modulation of downstream GPi β oscillations.

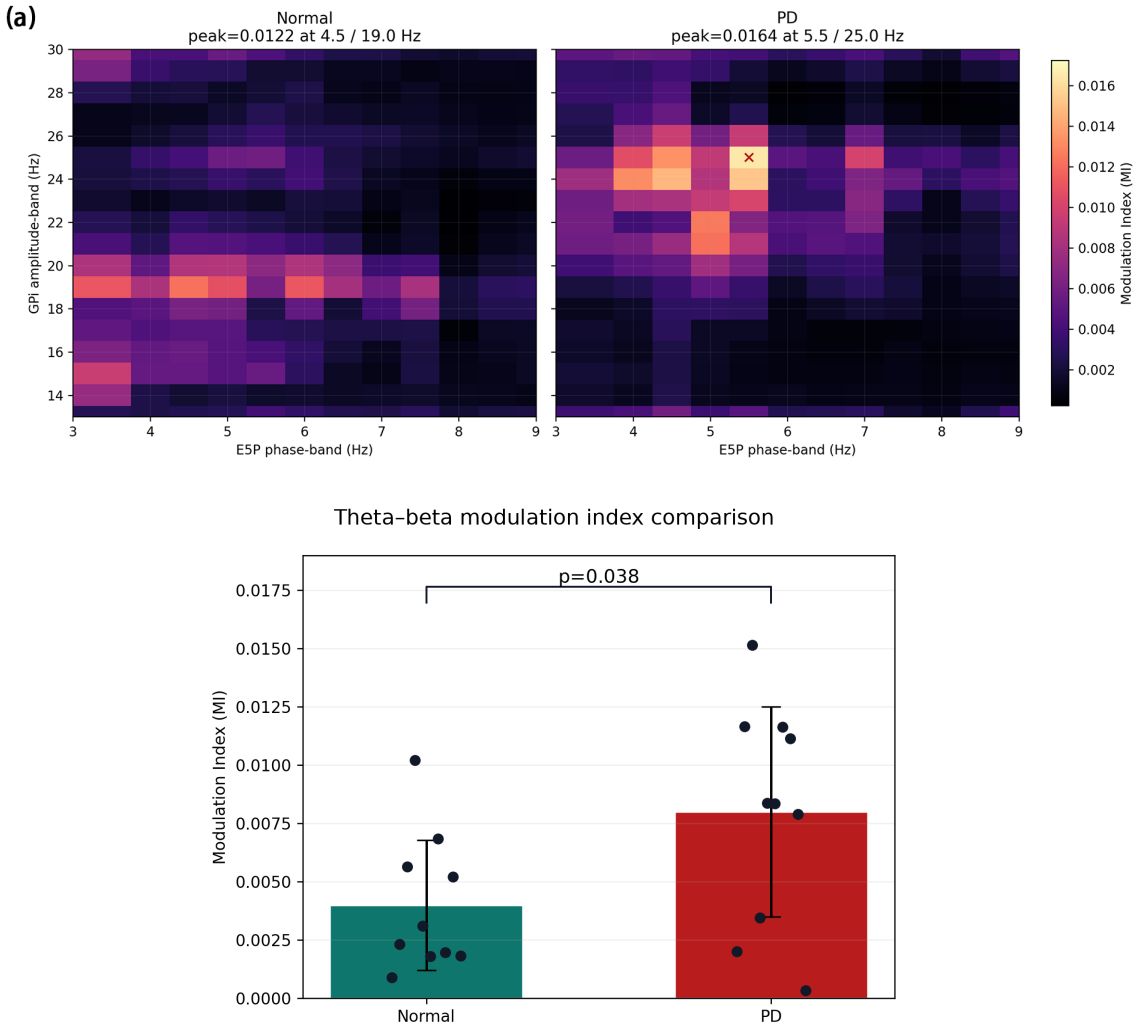

Figure 7. Comodulogram of cross-regional PAC between E5P phase and GPi amplitude. **(a)** Comodulogram heat maps for normal (left, peak MI = 0.0122 at 4.5/19.0 Hz) and PD (right, peak MI = 0.0164 at 5.5/25.0 Hz) states. **(b)** Bar chart comparing the mean θ–β MI between these two conditions.

Figure 8 shows the normalized mean GPi beta amplitude as a function of E5P theta phase. In the normal state, the distribution fluctuates around the uniform level with relatively small deviations. However, in the PD state, the distribution becomes markedly nonuniform. The GPi beta amplitude is maximal near 0°–60° of the E5P theta cycle. It decreases to a minimum near 220°–240°. This indicates that GPi β oscillations are preferentially expressed during a specific phase window of the E5P θ cycle. Biologically, this suggests that cortical theta acts as a temporal gating signal.

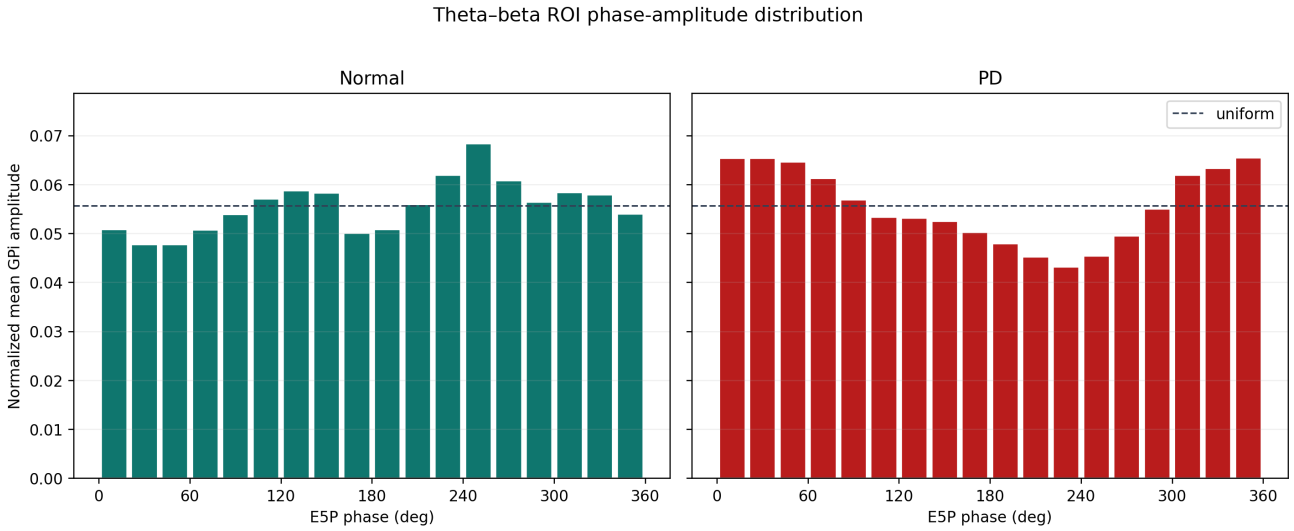

Figure 8. Phase-amplitude distribution for the θ–β frequency pair. Normalized mean GPi beta amplitude is plotted against E5P theta phase (18 bins). Left: Normal state. Right: PD state. The dashed line indicates the uniform distribution level.

3.3. Pathway dependence and temporal directionality

The preceding results establish the existence of cross-regional θ–β PAC. We now investigate whether this coupling is a mere coincidence or reflects pathway-dependent descending modulation.

Figure 9 shows the time-lag MI curve. At negative lags ($\tau < -50$ ms), the MI remains near baseline. As τ increases toward zero, the MI rises steeply. The peak MI value of approximately 0.0105 occurs at $\tau \approx +20$ ms. Beyond the peak, the MI decays gradually, returning to baseline by approximately $\tau = +75$ ms. The positive peak lag indicates that E5P θ phase temporally precedes the modulation of GPi β amplitude by approximately 20 ms, which supports the hypothesis that cortical E5P theta exerts a descending modulatory influence on GPi beta oscillations.

To identify which pathway mediates the descending θ–β PAC, we perform selective pathway blockade experiments. Three blockade conditions are tested (Figure 10): (1) cut E5A→D1-MSN (direct pathway), (2) cut E5P→D2-MSN (indirect pathway), and (3) cut E5P→STN (hyperdirect pathway). Each blockade is implemented by setting the corresponding synaptic conductance to zero while keeping the remaining pathways intact. Three outcome measures are examined: GPi β power, fixed-band MI (E5P θ phase × GPi β amplitude), and E5P-GPi beta-band coherence.

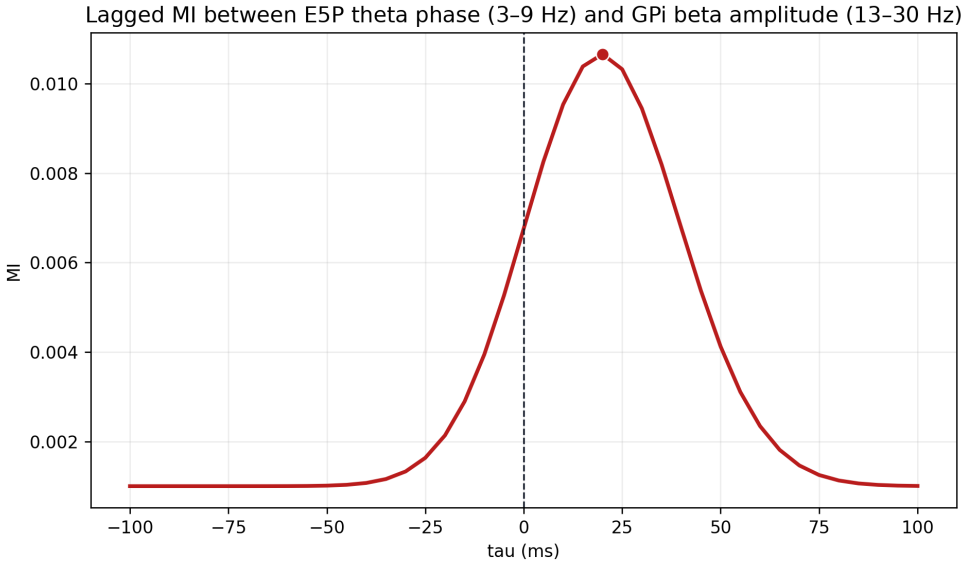

Figure 9. Time-lag MI between E5P θ phase and GPi β amplitude. The MI is plotted as a function of the time lag τ (-100 to $+100$ ms). The dashed vertical line marks $\tau = 0$.

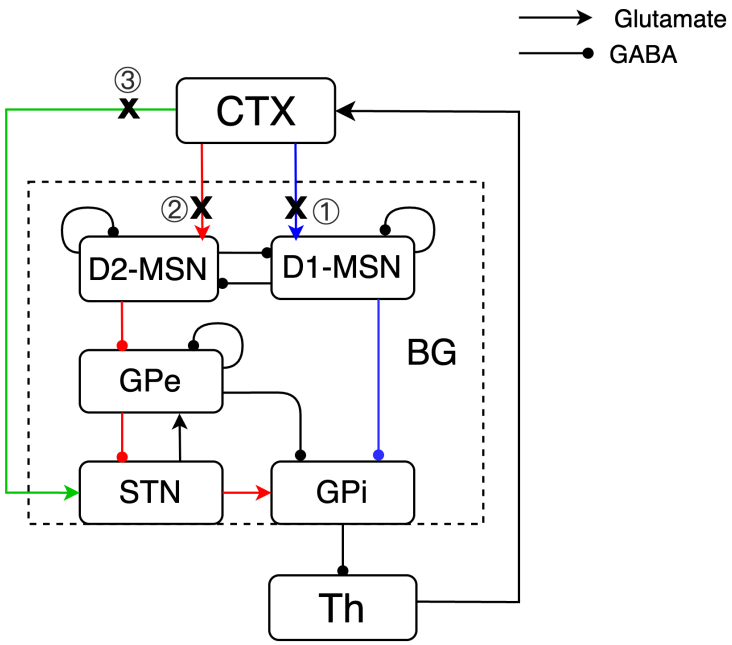

Figure 10. Network configuration for pathway blockade experiments. Three pathways are selectively disrupted: (1) E5A→D1-MSN (direct, blue), (2) E5P→D2-MSN (indirect, red), (3) E5P→STN (hyperdirect, green).

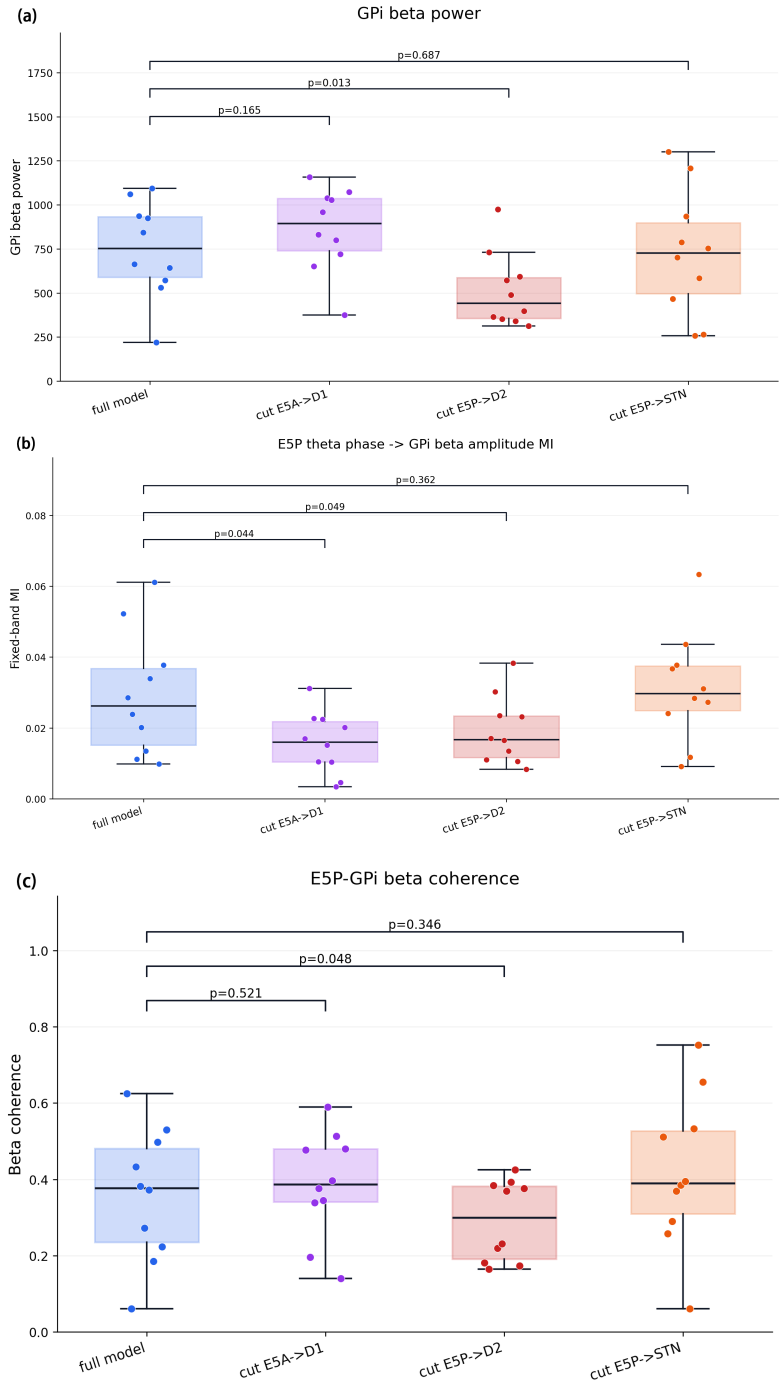

Figure 11. Effects of pathway blockade on GPi dynamics. **(a)** GPi beta power. **(b)** Fixed-band MI. **(c)** E5P-GPi beta coherence.

Figure 11 presents the effects of the selective pathway blockade across 10 paired simulation trials. For Figure 11(a), blocking E5A→D1 and E5P→STN produces little change ($p = 0.165$ and $p = 0.687$, respectively). In contrast, blocking E5P→D2 causes a dramatic reduction ($p = 0.013$). This indicates

that the indirect pathway is the primary route through which cortical activity sustains GPi beta oscillations at the current working point. For Figure 11(b), both the E5A→D1-MSN blockade and the E5P→D2-MSN blockade reduced the coupling strength ($p = 0.044$ and $p = 0.049$, respectively), whereas the E5P→STN blockade did not produce a significant effect ($p = 0.362$). The MI reduction under the E5P→D2 blockade confirms that the indirect pathway transmits both the oscillatory power and the phase–amplitude coupling relationship. And for Figure 11(c), only the E5P→D2-MSN blockade caused a significant reduction ($p = 0.048$); the effects of the E5A→D1-MSN and E5P→STN blockade were not significant ($p = 0.521$ and $p = 0.346$, respectively).

Taken together, the three measures converge on the same conclusion: The indirect pathway is the primary conduit for transmitting cortical theta modulation to GPi, which drives GPi beta oscillations with a phase-dependent temporal structure.

3.4. Modulating cortical theta to alleviate abnormal beta oscillations in GPi

The preceding sections have established that cross–regional θ-β PAC emerges under PD conditions, that this coupling is temporally directed with E5P leading GPi, and that it depends primarily on the indirect pathway. So, can targeted modulation of cortical theta activity reduce pathological GPi beta oscillations? We propose two intervention strategies. **Method 1: Block E5P→D2 (pathway intervention). Method 2: Attenuate E5P theta power (source intervention).** The theta-band rhythmicity of E5P neurons is reduced by modifying the intrinsic dynamics of E5P. Both interventions are evaluated using two outcome measures: GPi beta power (13–30 Hz) and fixed-band MI ($\phi_{\mathrm{E5P,3\text{-}9\,Hz}}$, $A_{\mathrm{GPi,13–30\,Hz}}$).

Figure 12 summarizes the effects of two intervention strategies across 10 paired simulation trials. For Figure 12(a), attenuating E5P theta activity significantly reduced GPi beta power compared with the full model ($p = 0.042$), whereas blocking the E5P→D2-MSN pathway showed a trend-level reduction ($p = 0.055$). This suggests that weakening the upstream cortical theta source can effectively suppress downstream GPi beta activity. For Figure 12(b), blocking the E5P→D2-MSN pathway significantly reduced E5P theta phase–GPi beta amplitude coupling ($p = 0.048$), whereas attenuating E5P theta activity did not produce a significant reduction in MI across trials ($p = 0.526$). These results suggest that a pathway blockade more directly disrupts the phase–amplitude coupling relationship, whereas source attenuation mainly reduces the downstream beta power. Therefore, the two interventions affect different aspects of the pathological theta–beta interaction.

The difference between the two interventions is informative. The pathway blockade (Method 1) reduces GPi beta by removing one transmission route, but the cortical theta source remains active and may still partially influence GPi through the remaining pathways. Source attenuation (Method 2) reduces GPi beta more strongly because it weakens the upstream rhythm that organizes downstream beta recruitment across the entire cortico-BG transmission architecture. This graded relationship supports a hierarchical model of GPi beta abnormality, in which the cortical theta rhythm provides the upstream temporal scaffold, the indirect pathway serves as the primary transmission axis, and the BG circuit amplifies and sustains the oscillation locally. Disrupting any level of this hierarchy reduces the pathological output, but weakening the source rhythm exerts the stronger overall effect.

From a therapeutic perspective, these results suggest three implications. First, treatment of GPi beta abnormality should not be limited to passive suppression of the output nucleus; the upstream cortical driving source should also be considered. Second, the E5P→D2 transmission axis emerges as

a mechanistically relevant target for pathway-oriented intervention, and cortical theta itself represents a potential source-level target for neuromodulation. Third, cortical theta power and its coupling with GPi beta (as measured by MI) may serve as real-time biomarkers for closed-loop neurostimulation systems, complementing the currently used beta power alone [9].

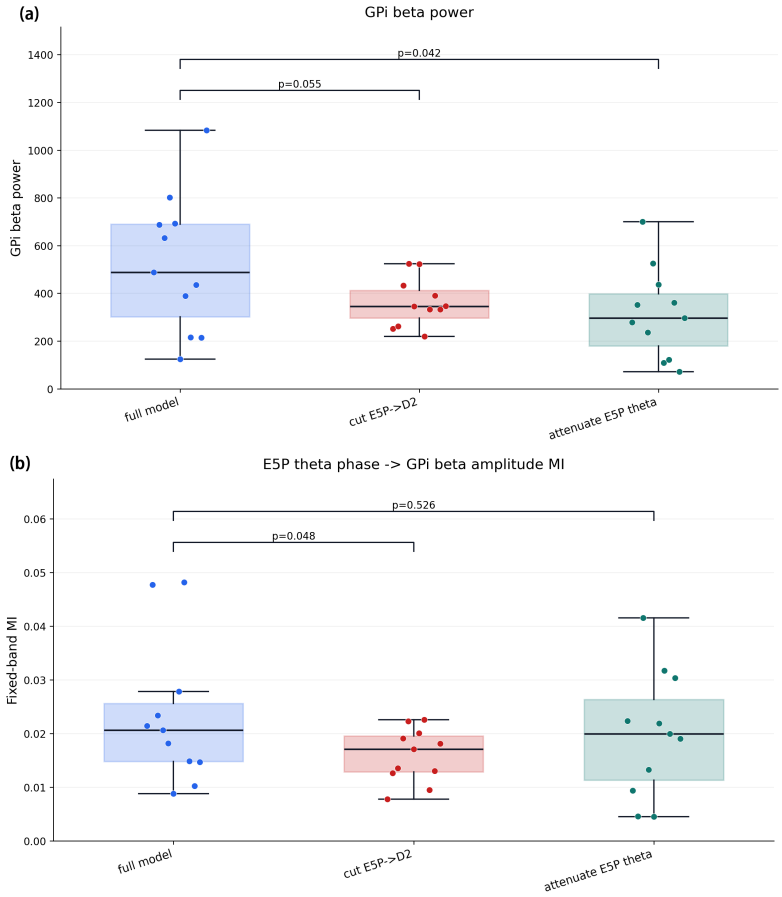

Figure 12. Effects of two intervention strategies on GPi beta oscillations (box plots, $n = 10$ trials). **(a)** GPi beta power. **(b)** Fixed-band MI (E5P theta phase → GPi beta amplitude).

4. Conclusions and discussion

In this study, we constructed a layered CTX-BG-Th network model. Using this model, we investigated cross-regional phase–amplitude coupling between cortical E5P θ oscillations and GPi β oscillations. The main findings are as follows.

Under PD conditions, the theta-band phase of E5P cortical neurons significantly modulates the beta-band amplitude of GPi neurons. Comodulogram analysis reveals a PAC hotspot centered at approximately 5.5 Hz (phase) and 25 Hz (amplitude). GPi beta amplitude peaks near 0°–60° of the E5P theta cycle and reaches a minimum near 220°–240°. Time-lag MI analysis shows that the coupling peaks at $\tau \approx +20$ ms, indicating that E5P θ phase leads GPi β amplitude changes. This temporal asymmetry supports a descending cortical-to-GPi modulatory direction. Pathway

blockade experiments further reveal that the indirect pathway is the primary conduit for this coupling. Two intervention strategie, blocking the E5P→D2 pathway and attenuating E5P theta power, both effectively reduce GPi beta oscillations and the associated PAC. Source attenuation (theta weakening) produces a larger reduction (~45%) than a pathway blockade alone (~28%), indicating that GPi beta abnormality has a hierarchical origin with cortical theta as the upstream driving rhythm.

The emergence of cross-regional θ–β PAC in the PD state can be understood through the interplay of three factors. First, dopamine depletion disinhibits E5P neurons and enhances their intrinsic theta-band rhythmicity. The IB-type dynamics of E5P neurons, which include a high-threshold L-type calcium current, produce burst firing that is naturally modulated at theta frequencies. Second, dopamine depletion alters striatal excitability (reduced M-type potassium conductance) and GPe lateral inhibition, creating conditions that favor synchronized beta oscillations within the STN-GPe-GPi circuit. Third, the E5P→D2-MSN projection links these two phenomena: Cortical theta periodically activates D2-MSNs, which periodically inhibit the GPe, which periodically releases STN from inhibition, producing theta-locked beta bursts in the GPi.

The present study provides several new findings on pathological oscillations in the cortico-basal ganglia loop. We show that θ–β phase–amplitude coupling can arise between the cortex and GPi, extending PAC beyond a local circuit phenomenon. The results also suggest that the indirect pathway plays an important role in transmitting cortical rhythmic activity to influence GPi beta oscillations. Finally, the intervention results show that both reducing cortical theta activity and weakening its transmission pathway can attenuate pathological GPi beta oscillations. Together, these findings connect abnormal coupling, pathway function, and possible intervention targets.

Our results suggest that treatment of GPi beta abnormality should not be limited to suppression of the BG output nucleus. The model indicates that cortical E5P theta activity may participate in the modulation of GPi beta oscillations. Therefore, the potential source-level target is the pathological E5P-related theta rhythm and its coupling with GPi beta activity. In principle, noninvasive neuromodulation techniques, such as transcranial magnetic stimulation (TMS) or transcranial alternating current stimulation (tACS), may provide possible routes for modulating cortical rhythms [27]. However, the concrete implementation of such modulation, including stimulation target, frequency, phase, intensity, and biomarker selection, remains to be determined experimentally. In addition, selective disruption of the E5P→D2 coupling axis may represent a pathway-level intervention strategy. Optogenetic approaches targeting specific cortical cell types and their striatal projections have shown promise in computational and experimental studies [20]. Furthermore, cortical θ power and its coupling with GPi beta, as measured by MI, may serve as candidate biomarkers for closed-loop DBS systems. These intervention-related implications should be interpreted as theoretical predictions and require further experimental validation.

Several limitations should be noted. The present study focuses on a representative Parkinsonian operating point and does not systematically examine the progressive process of dopamine depletion. In biological PD, dopamine loss occurs gradually and may continuously reshape striatal excitability, pallidal inhibition, and STN-GPe-GPi beta synchronization. Therefore, the cross-regional theta-beta PAC identified here should be interpreted as a mechanistic prediction under a fixed PD condition rather than as a complete description of the entire dopamine-depletion process. Future work will further examine how different dopamine depletion levels affect the emergence, strength, frequency profile, and pathway dependence of cortical-GPi theta–beta PAC. In addition, the proposed intervention

strategies remain computational predictions. Although blocking the E5P-D2 pathway and attenuating E5P theta activity reduce GPi beta oscillations in the model, the present study lacks direct support from experimental or clinical electrophysiological data. Therefore, these intervention-related findings should be interpreted as theoretical predictions, and further experimental validation is needed to determine. Future work may also compare the present physiologically constrained CTX-BG-Th loop with reduced nonlinear network motifs, such as Hindmarsh–Rose neuron chains, which have been used to study oscillation transfer and rhythm regularization in coupled neuronal systems [44].

Use of AI tools declaration

The authors declare they have not used Artificial Intelligence (AI) tools in the creation of this article.

Acknowledgments

This research was supported by the National Natural Science Foundation of China (Grant No.12272062).

Conflict of interest

The authors declare there are no conflicts of interest.

References

1. A. M. Graybiel, The basal ganglia, *Curr. Biol.*, **10** (2000), R509–R511. https://doi.org/10.1016/S0960-9822(00)00593-5
2. J. W. Mink, The basal ganglia: focused selection and inhibition of competing motor programs, *Prog. Neurobiol.*, **50** (1996), 381–425. https://doi.org/10.1016/S0301-0082(96)00042-1
3. M. R. DeLong, Primate models of movement disorders of basal ganglia origin, *Trends Neurosci.*, **13** (1990), 281–285. https://doi.org/10.1016/0166-2236(90)90110-V
4. Y. Smith, M. D. Bevan, E. Shink, J. P. Bolam, Microcircuitry of the direct and indirect pathways of the basal ganglia, *Neuroscience*, **86** (1998), 353–387. https://doi.org/10.1016/S0306-4522(98)00004-9
5. P. Brown, A. Oliviero, P. Mazzone, A. Insola, P. Tonali, V. Di Lazzaro, Dopamine dependency of oscillations between subthalamic nucleus and pallidum in Parkinson's disease, *J. Neurosci.*, **21** (2001), 1033–1038. https://doi.org/10.1523/JNEUROSCI.21-03-01033.2001
6. C. Hammond, H. Bergman, P. Brown, Pathological synchronization in Parkinson's disease: networks, models and treatments, *Trends Neurosci.*, **30** (2007), 357–364. https://doi.org/10.1016/j.tins.2007.05.004
7. E. Stein, I. Bar-Gad, Beta oscillations in the cortico-basal ganglia loop during parkinsonism, *Exp. Neurol.*, **245** (2013), 52–59. https://doi.org/10.1016/j.expneurol.2012.07.023
8. A. A. Kühn, A. Kupsch, G. H. Schneider, P. Brown, Reduction in subthalamic 8–35 Hz oscillatory activity correlates with clinical improvement in Parkinson's disease, *Eur. J. Neurosci.*, **23** (2006), 1956–1960. https://doi.org/10.1111/j.1460-9568.2006.04717.x

9. S. Little, A. Pogosyan, S. Neal, B. Zavala, L. Zrinzo, M. Hariz, et al., Adaptive deep brain stimulation in advanced Parkinson disease, *Ann. Neurol.*, **74** (2013), 449–457. https://doi.org/10.1002/ana.23951
10. A. Nambu, H. Tokuno, M. Takada, Functional significance of the cortico-subthalamo-pallidal 'hyperdirect' pathway, *Neurosci. Res.*, **43** (2002), 111–117. https://doi.org/10.1016/S0168-0102(02)00027-5
11. R. L. Albin, A. B. Young, J. B. Penney, The functional anatomy of basal ganglia disorders, *Trends Neurosci.*, **12** (1989), 366–375. https://doi.org/10.1016/0166-2236(89)90074-X
12. R. T. Canolty, R. T. Knight, The functional role of cross-frequency coupling, *Trends Cognit. Sci.*, **14** (2010), 506–515. https://doi.org/10.1016/j.tics.2010.09.001
13. O. Jensen, L. L. Colgin, Cross-frequency coupling between neuronal oscillations, *Trends Cognit. Sci.*, **11** (2007), 267–269. https://doi.org/10.1016/j.tics.2007.05.003
14. A. B. L. Tort, R. Komorowski, H. Eichenbaum, N. Kopell, Measuring phase-amplitude coupling between neuronal oscillations of different frequencies, *J. Neurophysiol.*, **104** (2010), 1195–1210. https://doi.org/10.1152/jn.00106.2010
15. C. de Hemptinne, E. S. Ryapolova-Webb, E. L. Air, P. A. Garcia, K. J. Miller, J. G. Ojemann, et al., Exaggerated phase-amplitude coupling in the primary motor cortex in Parkinson disease, *Proc. Natl. Acad. Sci. U.S.A.*, **110** (2013), 4780–4785. https://doi.org/10.1073/pnas.1214546110
16. C. de Hemptinne, N. C. Swann, J. L. Ostrem, E. S. Ryapolova-Webb, M. Luciano, N. B. Galifianakis,et al., Therapeutic deep brain stimulation reduces cortical phase-amplitude coupling in Parkinson's disease, *Nat. Neurosci.*, **18** (2015), 779–786. https://doi.org/10.1038/nn.3997
17. J. Zheng, K. L. Anderson, S. L. Leal, A. Shestyuk, G. Gulsen, L. Mnatsakanyan, et al., Amygdala-hippocampal dynamics during salient information processing, *Nat. Commun.*, **8** (2017), 14413. https://doi.org/10.1038/ncomms14413
18. B. Nandi, P. Swiatek, B. Kocsis, M. Ding, Inferring the direction of rhythmic neural transmission via inter-regional phase-amplitude coupling (ir-PAC), *Sci. Rep.*, **9** (2019), 6933. https://doi.org/10.1038/s41598-019-43272-w
19. Y. Yu, F. Han, Q. Wang, Exploring phase-amplitude coupling from primary motor cortex-basal ganglia-thalamus network model, *Neural Networks*, **153** (2022), 130–141. https://doi.org/10.1016/j.neunet.2022.05.027
20. Y. Yu, Y. Fan, S. Hou, Q. Wang, Optogenetic stimulation of primary motor cortex regulates beta oscillations in the basal ganglia: A computational study, *Commun. Nonlinear Sci. Numer. Simul.*, **117** (2023), 106918. https://doi.org/10.1016/j.cnsns.2022.106918
21. S. Dura-Bernal, S. A. Neymotin, B. A. Suter, G. M. G. Shepherd, W. W. Lytton, Multiscale dynamics and information flow in a data-driven model of the primary motor cortex microcircuit, *Cell Rep.*, **42** (2023), 112574. https://doi.org/10.1016/j.celrep.2023.112574
22. S. A. Neymotin, S. Dura-Bernal, P. Lakatos, T. D. Sanger, W. W. Lytton, Multitarget multiscale simulation for pharmacological treatment of dystonia in motor cortex, *Front. Pharmacol.*, **7** (2016), 157. https://doi.org/10.3389/fphar.2016.00157

23. B. Bai, X. Shi, Z. Li, The effects of cortical inputs on the oscillation and synchronization of the basal ganglia, *Physica A*, **677** (2025), 130900. https://doi.org/10.1016/j.physa.2025.130900
24. A. Sirota, S. Montgomery, S. Fujisawa, Y. Isomura, M. Zugaro, G. Buzsáki, Entrainment of neocortical neurons and gamma oscillations by the hippocampal theta rhythm, *Neuron*, **60** (2008), 683–697. https://doi.org/10.1016/j.neuron.2008.09.014
25. J. E. Lisman, O. Jensen, The theta-gamma neural code, *Neuron*, **77** (2013), 1002–1016. https://doi.org/10.1016/j.neuron.2013.03.007
26. K. D. Harris, G. M. G. Shepherd, The neocortical circuit: themes and variations, *Nat. Neurosci.*, **18** (2015), 170–181. https://doi.org/10.1038/nn.3917
27. C. F. Underwood, L. C. Parr-Brownlie, Primary motor cortex in Parkinson's disease: Functional changes and opportunities for neurostimulation, *Neurobiol. Dis.*, **147** (2021), 105159. https://doi.org/10.1016/j.nbd.2020.105159
28. K. Kumaravelu, D. T. Brocker, W. M. Grill, A biophysical model of the cortex-basal ganglia-thalamus network in the 6-OHDA lesioned rat model of Parkinson's disease, *J. Comput. Neurosci.*, **40** (2016), 207–229. https://doi.org/10.1007/s10827-016-0593-9
29. S. Dura-Bernal, S. A. Neymotin, B. A. Suter, G. M. G. Shepherd, W. W. Lytton, Multiscale dynamics and information flow in a data-driven model of the primary motor cortex microcircuit, *BioRxiv*, 2017. https://doi.org/10.1101/201707
30. M. Pospischil, M. Toledo-Rodriguez, C. Monier, Z. Piwkowska, T. Bal, Y. Frégnac, et al., Minimal Hodgkin-Huxley type models for different classes of cortical and thalamic neurons, *Biol. Cybern.*, **99** (2008), 427–441. https://doi.org/10.1007/s00422-008-0263-8
31. E. M. Izhikevichl, *Dynamical Systems in Neuroscience: The Geometry of Excitability and Bursting*, MIT Press, Cambridge, MA, 2006. https://doi.org/10.7551/mitpress/2526.001.0001
32. I. Reuveni, A. Friedman, Y. Amitai, M. Gutnick, Stepwise repolarization from Ca^{2+} plateaus in neocortical pyramidal cells: evidence for nonhomogeneous distribution of HVA Ca^{2+} channels in dendrites, *J. Neurosci.*, **13** (1993), 4609–4621. https://doi.org/10.1523/JNEUROSCI.13-11-04609.1993
33. A. Destexhe, T. Bal, D. A. McCormick, T. J. Sejnowski, Ionic mechanisms underlying synchronized oscillations and propagating waves in a model of ferret thalamic slices, *J. Neurophysiol.*, **76** (1996), 2049–2070. https://doi.org/10.1152/jn.1996.76.3.2049
34. D. Terman, J. E. Rubin, A. C. Yew, C. J. Wilson, Activity patterns in a model for the subthalamopallidal network of the basal ganglia, *J. Neurosci.*, **22** (2022), 2963–2976. https://doi.org/10.1523/JNEUROSCI.22-07-02963.2002
35. R. Q. So, A. R. Kent, W. M. Grill, Relative contributions of local cell and passing fiber activation and silencing to changes in thalamic fidelity during deep brain stimulation and lesioning: a computational modeling study, *J. Comput. Neurosci.*, **32** (2012), 499–519. https://doi.org/10.1007/s10827-011-0366-4
36. H. Kita, T. Kita, Cortical stimulation evokes abnormal responses in the dopamine-depleted rat basal ganglia, *J. Neurosci.*, **31** (2011), 10311–10322. https://doi.org/10.1523/JNEUROSCI.0915-11.2011

37. H. Nakanishi, H. Kita, S. T. Kitai, Intracellular study of rat substantia nigra pars reticulata neurons in an in vitro slice preparation: electrical membrane properties and response characteristics to subthalamic stimulation, *Brain Res.*, **437** (1987), 45–55. https://doi.org/10.1016/0006-8993(87)91525-3

38. H. Kita, S. T. Kitai, Intracellular study of rat globus pallidus neurons: membrane properties and responses to neostriatal, subthalamic and nigral stimulation, *Brain Res.*, **564** (1991), 296–305. https://doi.org/10.1016/0006-8993(91)91466-E

39. K. Fujimoto, H. Kita, Response characteristics of subthalamic neurons to the stimulation of the sensorimotor cortex in the rat, *Brain Res.*, **609** (1993), 185–192. https://doi.org/10.1016/0006-8993(93)90872-K

40. J. Baufreton, E. Kirkham, J. F. Atherton, A. Menard, P. J. Magill, J. P. Bolam, et al., Sparse but selective and potent synaptic transmission from the globus pallidus to the subthalamic nucleus, *J. Neurophysiol.*, **102** (2009), 532–545. https://doi.org/10.1152/jn.00305.2009

41. M. A. Farries, H. Kita, C. J. Wilson, Dynamic spike threshold and zero membrane slope conductance shape the response of subthalamic neurons to cortical input, *J. Neurosci.*, **30** (2010), 13180–13191. https://doi.org/10.1523/JNEUROSCI.1909-10.2010

42. N. Mallet, A. Pogosyan, A. Sharott, J. Csicsvari, J. P. Bolam, P. Brown, et al., Disrupted dopamine transmission and the emergence of exaggerated beta oscillations in subthalamic nucleus and cerebral cortex, *J. Neurosci.*, **28** (2008), 4795–4806. https://doi.org/10.1523/JNEUROSCI.0123-08.2008

43. A. V. Cruz, N. Mallet, P. J. Magill, P. Brown, S. D. Averbeck, Effects of dopamine depletion on information flow between the subthalamic nucleus and external globus pallidus, *J. Neurophysiol.*, **106** (2011), 2012–2023. https://doi.org/10.1152/jn.00094.2011

44. M. La Rosa, M. I. Rabinovich, R. Huerta, H. D. I. Abarbanel, L. Fortuna, Slow regularization through chaotic oscillation transfer in an unidirectional chain of hindmarsh–rose models, *Phys. Lett. A*, **266** (2000), 88–93. https://doi.org/10.1016/S0375-9601(00)00015-3

AIMS Press